Structural Health Monitoring by Detection of Abrupt Changes in Response Using Wavelets: Application to a 6-story RC Building Damaged by an Earthquake

by

Maria I. Todorovska[1] and Mihailo D. Trifunac[2]

ABSTRACT

A signal processing method for structural health monitoring is applied to detect damage in the former Imperial County Services (ICS) Building, caused by the 1979 Imperial Valley earthquake in southern California. The building response was recorded by a 13-chanel array of accelerometers, and a description of the distribution of the damage throughout the structure is available. The method is based on detecting abrupt changes in the seismic vibration response by analysis of the finest detail coefficients of a wavelet basis expansion of the recorded response. This method has been previously proven to work for numerically simulated response of simple models with postulated damage, but not for real earthquake data. The analysis in this paper critically examines the capabilities of this method to detect damage in real data. The analysis shows that most of the detected prominent abrupt changes are consistent with the spatial distribution and severity of the reported damage. Other less prominent abrupt changes can be explained by high frequency energy pulses of the input motion that propagated through the building. There are also few prominent abrupt changes that remain unexplained at this time. It is concluded that this method could provide useful information for structural health monitoring and for understanding the seismic response of structures and the occurrence of damage. Further investigations are needed of the "noise" of the method, how to distinguish those abrupt changes not caused by damage, and how to relate the magnitude of the detected abrupt changes to the level of damage.

KEYWORDS: structural health monitoring; damage detection; wavelets; Imperial County Services Building.

1.0 INTRODUCTION

Structural health monitoring is an important and challenging problem in earthquake engineering. It refers to *"the process of determining and tracking structural integrity and assessing the nature of damage in a structure"* (Chang et al. 2003). A recent review of research on this topic can be found in Chang et al. (2003), and a detailed review of methods for structural and mechanical systems, based on changes in their vibration characteristics, can be found in Doebling et al. (1996).

Most of the vibration-based health monitoring methods used in civil engineering are based on detecting shifts in natural frequencies or changes in the mode shapes, determined from seismic or ambient monitoring data. To be detectable, these changes have to be larger than the changes due to other environmental factors (e.g. temperature and soil-structure interaction) referred to as "noise" in the method. In the case of earthquake damage,

[1] Research Professor, Dept. of Civil Engineering, University of Southern California, Los Angeles, CA 90089-2531, USA, E-mail: mtodorov@usc.edu
[2] Professor, Dept. of Civil Engineering, University of Southern California, Los Angeles, CA 90089-2531, USA, E-mail: trifunac@usc.edu

significant factors affecting the efficiency of detecting changes in the natural frequency and associating them with damage are: (1) the high level of redundancy of the structures, which results in small changes in the overall stiffness when the damage is localized, and (2) shifts in frequency due to soil-structure interaction. The latter are often mistakenly interpreted as damage, and are difficult to separate in analyses of earthquake response data, due to inadequate number and distribution of sensors (Trifunac et al., 1996a,b). Other factors include (3) the effect of gravity and friction in the use of ambient vibration data (Ivanović et al., 1999). The changes in the mode shapes (e.g. curvature) are less sensitive to such factors, but are more difficult to detect and require more extensive instrumentation than what is usually available in instrumented buildings (Chang et al. 2003; Trifunac and Todorovska 2001). Other difficulties in the vibration based methods include: (4) reliance on baseline data, for which just a model based estimate may be available, or a measurement under different environmental conditions, and (5) reliance on a model and analytical tools for prediction of response, which are idealizations of and may differ significantly from the real structure and its behavior.

The time dependent nonparametric identification methods, e.g., Hilbert transform method, or some "moving window" method such as wavelet and Gabor transform methods (Todorovska 2001) for estimation of instantaneous frequency, avoid the dependence on a model and baseline data, by detecting *changes* in frequency during the cause of earthquake shaking. The time resolution of the window based methods, however, depends on the length of the time window, which cannot be arbitrarily small (as the time window becomes smaller, the time resolution increases, but the frequency resolution decreases, and for meaningful identification, the time window should be long enough to contain at least few cycles of the period being estimated). This also limits the earliest time that the instantaneous frequency can be estimated (to half of the length of the window). Hilbert transform method is literally instantaneous, but is very sensitive to noise. Also, these methods are based on the asymptoticity assumption and do not give accurate results in time intervals where the amplitude envelope of the signal changes rapidly.

More recent vibration based methods include statistical pattern recognition (Sohn and Law 1999) and artificial neural networks. The former does rely on an analytical model for prediction of response for various scenarios of damage, and is based on matching (in statistical sense) patterns in observed response data with patterns in estimated response for various damage scenarios. The latter method relies on training with data that correspond to different scenarios of damage, and search in a large set of training data (each corresponding to some scenario of damage) for the pattern that matches the observed pattern. The convergence, however, depends on the exhaustiveness of the training data set, and is not guaranteed (Chang et al. 2003).

Another recent method, which is the subject of this paper, involves detection of sudden changes in structural response data using wavelet analysis. This method is nonparametric and allows accurate estimation of the time of the sudden change, benefiting from the fine time resolution of the wavelet transform at small scales (i.e. high frequencies). An advantage of the method is that it is *nonparametric* and does not rely on baseline data. Another advantage is that it does not depend on the change of the structural frequency, which is sensitive to soil-structure interaction. The remaining part of this section presents a literature review on its previous applications, which are mostly on numerically simulated data.

Sone et al. (1995) explored this method on *numerically simulated* time history of the response of a single degree-of-freedom system with stationary noise, and damage represented as fatigue caused by reduction of stiffness. They used decomposition in a basis of db4 Daubechies wavelets, and concluded that, even for noise-contaminated signals, wavelet analysis leads to a good estimation of the occurrence times of the postulated damage.

Wang and Deng (1998), also using *numerically simulated* response data, explored the use of wavelets for detection of the spatial location of damage within a beam with a short transverse crack, under static and dynamic loading conditions. They used Haar wavelets to analyze a set of *numerically simulated* "measurements" at various locations within the beam, and concluded that the location of the crack could be well detected, with resolution depending on the spatial resolution of the "measurements."

Vincent et al. (1999) also used *numerically simulated* response data to detect damage in a three-story shear building subjected to a sinusoidal excitation, with damage introduced as a sudden loss of stiffness in the first story columns. They concluded that discrete wavelet analysis has the capability to identify signal singularities such as sharp changes in acceleration resulting from sudden damage.

Another study based on *numerically simulated* data was carried out by Corbin et al. (2000), who studied response of: (i) a three degree-of-freedom system with breakable springs connected in parallel, (ii) a cantilever beam, and (iii) a finite element model of a building. Damage was introduced either by breaking the springs or by removal of stiffness components at a specified moment. They concluded that the damage and the moment when it occurs could be detected by spikes in the plots of higher resolution details from wavelet decomposition of acceleration response.

Rezai et al. (1998) applied this method to *actual earthquake response data*, i.e. the acceleration responses recorded in a 7-story reinforced concrete building in Van Nuys in the Los Angeles metropolitan area damaged by the 1994 Northridge earthquake. They analyzed the distribution of the amplitude of the wavelet coefficients in the highest frequency subband of wavelet decomposition in a Haar basis for two earthquakes that damaged the building—the 1971 San Fernando and the 1994 Northridge. They identified time intervals with larger values of these coefficients, and they interpreted these large values to be due to "severe abrupt changes in the frequency content of the signals," which result from damage. They concluded that the technique might suggest the time when damage occurred. Their analysis did not consider and exclude other possible causes for the detected abrupt changes.

Hou et al. (2000) explored the method using both *numerically simulated response* and recorded earthquake response. They analyzed (i) a simple structural model represented by a single degree-of-freedom system with breakable springs connected in parallel, and (ii) the record of the 1971 San Fernando earthquake at the roof of a building in the Los Angeles area, which was damaged by this earthquake. In case (i), damage was introduced by braking the springs, after certain number of cycles or when a certain value of response was reached. In case (ii) the damage consisted of cracks and spalling of the columns and girders. They concluded that the structural damage or change in the system stiffness may be detected by spikes in the details of the wavelet decomposition of the response data (acceleration) at the roof, and that the location of these spikes may accurately indicate the moments when the structural damage occurred. However, as with Rezai et al. (1998), their analysis of the actual earthquake response data only shows that that *there are* spikes in the wavelet coefficients in earthquake response data of buildings known to have been damaged, but do not show that these spikes have been caused by damage. They recommended "*further experimental laboratory studies and field inspections on damaged structures are needed to justify the results and bring this approach into practical application*." They also studied the influence of stationary noise in the signals and concluded that that damage is more detectable if the level of noise is weaker.

Hera and Hou (2004) applied this method to *numerically simulated* acceleration response data (by a finite element code), and used expansion in a basis of Daubechies db4 wavelets. They concluded that sudden damage and the time when it occurred could be detected, and that the damaged region could also be determined.

Another related study is by Ovanesova and Suárez (2004), who explored the use of *spatial wavelet transform* to detect the location of damage in a theoretical model of a fixed-end beam under static and dynamic loading, and in a simple plane frame with a cracked column subjected to horizontal and vertical loads. They considered two cases of location of the crack—one far from the column-beam joint, and the other one near to the joint. They concluded that the effectiveness of the spatial wavelet analysis is sensitive to the boundary conditions of the members and the distance from the structural supports and joints.

This paper critically examines the success of this method to detect damage in *actual earthquake response* data, by studying a well-instrumented building that has been damaged, and considering other causes of the detected abrupt changes. The case study is the former Imperial County Services Building in El Centro in southern California, which was severely damaged by the 1979 Imperial Valley earthquake and was later demolished. This paper shows results of analysis of the acceleration response. Further details about this study, and application to different measures of absolute and relative response can be found in Todorovska and Trifunac (2005).

2.0 METHODOLOGY

The theoretical framework for construction of wavelet bases – multiresolution analysis – was postulated by Mallat (1989), who saw the connection between wavelet analysis and subband decomposition. Multiresolution analysis consists of splitting a signal $f[n]$ into higher and lower frequency components, $D_1(t)$ and $A_1(t)$, by application respectively of a high pass and a low pass filter $H_1(\omega)$ and $H_2(\omega)$, and recursively repeating this to the output of the low frequency filter

$$\begin{aligned} f(t) &= A_1(t) + D_1(t) \\ &= A_2(t) + D_2(t) + D_1(t) \\ &= A_3(t) + D_3(t) + D_2(t) + D_1(t) \\ &= .... \end{aligned} \qquad (1)$$

After J steps, the output consist of a series of high frequency subbands, $D_j(t)$, $j = 1,...,J$, containing the *detail* of the signal at different resolutions, and the last low frequency subband, A_J, containing a *smooth approximation* of the signal at the lowest resolution level considered, J. The smooth approximation shows the *trend* in the data, while the detail subbands shows novelties, or "surprises" in the data (e.g. abrupt changes), viewed at different resolution levels, with subband $D_1(t)$ containing the finest detail. Multiresolution analysis guarantees the existence of bases of wavelets at each resolution level, $\{\psi_{j,k}\}_{j,k\in\mathbb{Z}}$, and a basis of scaling functions, $\{\varphi_{J,k}\}_{k\in\mathbb{Z}}$, to further expand the detail subbands, and the last smooth subband, as follows

$$D_j(t) = \sum_{k=1}^{N/2^j} d_{j,k}\psi_{j,k}(t) \qquad (2)$$

and

$$A_J(t) = \sum_{k=1}^{N/2^J} a_{J,k}\varphi_{J,k}(t) \qquad (3)$$

The coefficients of expansion are in fact the wavelet transforms of the signal with respect to the particular wavelet in the basis (or its dual in the case of bi-orthogonal wavelets). For discrete time signals and wavelet bases with compact support, they can be efficiently computed by the pyramid algorithm, which is asymptotically faster even than the FFT. Further details about wavelet analysis can be found in various textbooks on wavelets (e.g. Vetterli and Kovacević 1995).

An abrupt change, e.g. an impulse or a step function at some point in time, will result in large wavelet coefficients of the detail subbands corresponding to the wavelets that are centered near that time. Such large coefficients will be referred to as "surprises." Although all the detail subbands will be affected, the surprises will be the largest in the finest resolution subband. Also, the high frequency energy in the structural response, which is "noise" for the method will have less energy in the highest frequency subband, $D_1(t)$. Hence, the health monitoring method consists of identifying such large amplitude coefficients in the highest frequency subband.

For this analysis, we chose a basis of bi-orthogonal wavelets (bior 6.8 wavelet), because they can be both symmetric and smooth, hence avoiding phase distortion, and smoothing smaller and spurious peaks in the wavelet coefficients, and emphasizing the most significant abrupt changes. We identify the "surprises" in the distribution of the *squared* coefficients of the level 1 detail subband, $d_{1,k}$, $k = 1,...N/2$, where N is the signal length, which represent the energy distribution in the subband 12.5 to 25 Hz for data sampled at 0.02 s (Todorovska and Hao 2003). We label by T1, T2, … those surprises believed to be due to damage (i.e. consistent with the distribution of reported damage), as G1, G2, … those believed to be due to high frequency pulses of the input motion that have propagated through the building (i.e. with amplitude and time delays consistent with wave propagation with velocity estimated from the building frequency), and as F1, F2, … those that we could not explain.

3.0 THE CASE STUDY

3.1 Description of the Building

The former Imperial County Services (ICS) building was a 6-story reinforced concrete structure located in the El Centro area in Southern California. It was designed in compliance with the 1967 Uniform Building Code, and its construction was completed in 1969. It had plan dimensions 41.70×26.02 m and height 25.48 m. Figure 1 shows its foundation and ground floor (top) and typical floor (bottom) layouts. The foundation system was composed of pile groups and pile caps directly located under the columns and walls. The pile caps were connected to each other by ground-level beams. Up to depth of 9 m, the underlying soil consisted of soft to medium-stiff damp sandy clay with organic materials, with inter-layers of medium dense moist sand, and beneath 9 m it consisted of stiff, moist sandy clay and silty clay.

The structure was made of reinforced concrete, with minimum ultimate compressive strength of 27.6 MPa—for the walls, beams and slabs, 34.5 MPa—for the columns, and 20.7 MPa—for the foundation elements, and reinforcement steel of 276 MPa. The structural configuration in the NS (transverse) direction consisted of two concrete panels at the east and west ends of the building (see Fig. 1), which extended only from the second floor to the roof, and were supported by cantilever parts of the frame beams, which extended in the EW direction. At the ground level, four panels were located between axis 2 and 3 along lines A and C through D. In the EW (longitudinal) direction, the structural system consisted of four beam-column frames. The facade columns had a variable cross-section, varying from rectangular to trapezoidal at the second floor (Kojić et al. 1984).

The 16-channel seismic monitoring array (installed by the California Division of Mines and Geology) consisted of a 13-channel structural array of force balance accelerometers (FBA-1) with a central analog recording system, and a tri-axial SMA-1 accelerometer in the "free field," approximately 104 m east from the northeast corner of the building. Figure 2 shows the location and orientation of the sensors. The sensors for channels 1 through 4 were attached under the roof slab, and for 5 through 13—on the topside of the floor slabs. The recording system had a horizontal starter on the roof (adjacent and parallel to channel 4), and a vertical starter on the ground floor (adjacent to channels 11, 12 and 13). A more detailed description of the structural system and seismic instrumentation can be found in Kojić et al. (1984).

The apparent frequencies of the ICS building, determined from ambient vibration tests carried out before the 1979 Imperial Valley earthquake, were 2.2–2.8 Hz for NS vibrations, and 1.5 Hz for EW vibrations (Pardoen 1979).

3.2 Earthquake Damage

The Imperial Valley earthquake of October 19, 1979 (M_L = 6.6, depth H=8 km) occurred on the Imperial Fault near El Centro in southern California, at epicental distance of about 26 km southeast from the building. From the hypocenter, the dislocation propagated northwest with velocity near 2.5 km/s, and after about 9 s it passed by the closest distance to the building, 7 km to southwest (Fig. 3; Jordanovski and Trifunac, 1990a,b). Thus, during the first 9 s, the building was receiving larger than average power of strong motion, due to strong directivity to northwest.

The building was severely damaged by this earthquake, and was later demolished (Kojić et al., 1984). Figure 4 shows a schematic representation of the main damage. The principal failures occurred in the columns of frame F (at the east end of the building) at the ground floor. The vertical reinforcement was exposed and buckled, and the core concrete could not be retained, resulting in shortening of the columns which caused cracking of the floor beams and slabs near column line F on the second, third and higher floors. Columns in lines A, B, D and E also suffered damage. Columns in frames A and E did not suffer such extensive damage as shortening and buckling of the reinforcement in line F at the east side, but large concrete cracks and exposed reinforcement could be seen near the base. In the columns in interior frames B through E, visible cracks and spalling of the concrete cover could be seen. A more detailed description of the damage and analysis of the response of the building can be found in Kojić et al. (1984).

3.3 Strong Motion Data

All 16 channels recorded the earthquake. The peak accelerations at the roof and ground floor were 571 cm/s^2 and 339 cm/s^2 in the NS direction and 461 cm/s^2 and 331 cm/s^2 in the EW direction. The film records were digitized and processed at USC (Trifunac and Lee, 1979) and the data released was sampled at 0.02 s, and band pass filtered between 0.1-0.125 and 25-27 Hz. Figure 5 shows the corrected accelerations.

4.0 RESULTS AND ANALYSIS

4.1 Drifts, Fourier and Time-Frequency Analyses

Figure 6 shows the average inter-story drifts between the roof and 2nd floor, and the drifts between the 2nd floor and ground level at the west end, center and the east end of the building. These drifts represent the sum of the drift due to *rigid body rocking* (one of the effects of soil-structure interaction) and drift due to *deformation* of the building, which could not be separated because of inadequate instrumentation. These drifts suggest (1) "soft" first story in both NS and EW directions, and (2) larger flexibility in the EW direction. In the EW direction, the drifts exceed 1.5%, and in the NS direction it exceeded 0.5%. The first story drifts are significantly larger at the ends than at the center, suggesting (3) significant torsional response, probably excited by the wave passage (Todorovska and Lee, 1999), and amplified by the asymmetric distribution of stiffness in the NS direction at the soft first story (see Figs 1 and 2). The first story drifts are larger at the east side, probably initially as a result of the smaller stiffness at that end, and later due to the larger damage.

Figure 7 shows Fourier spectra for the NS (left) and EW (right) responses of the roof acceleration (top), ground floor acceleration (middle) and relative displacement (bottom), all at the center of the building (the NS motion at the center of the ground floor was estimated by interpolation). This suggests a wide variation of the NS system frequency (0.7 to about 2 Hz), and EW system frequency near 0.6 Hz during most of the duration of shaking.

Figure 8 shows for the NS (left) and EW (right) responses the instantaneous system frequency (bottom) estimated from the ridge of the Gabor transform of the roof relative response with $\sigma = 1$ (Todorovska 2001), ground floor accelerations (top), and the roof displacements at the center of the building relative to the ground floor (middle). The relative roof displacement is a sum of the displacement due to rigid body rocking and due to deformation of the structure, which could not be separated. It can be seen that the NS frequency dropped from about 2 Hz to 0.8 Hz, and the EW frequency dropped from about 1 Hz to 0.6 Hz. Possible causes of these changes are the effect of the foundation soil, through the mechanism of soil-structure interaction, and degradation of stiffness due to damage, but the degree to which each of these causes contributed to the overall effect cannot be determined from the recorded response, due to inadequate number and location of sensors.

4.2 Detected Abrupt Changes and Analysis

Figures 9 shows squares coefficients of the detail subband of a level 1 wavelet basis decomposition of acceleration sampled at 0.02 s (corresponding to Nyquist frequency of 25 Hz). This subband spans (ideally) the frequency band 12.5 to 25 Hz. Parts a and b correspond respectively to NS and EW vibrations. In part a, the results are ordered so that the first three curves correspond to motions recorded at the west side of the building, the next three—at the center, and the last three—at the east side of the building. The shades highlight time intervals with large amplitude coefficients, i.e. "surprises." The instantaneous frequency is shown at the bottom.

4.2.1 Consistency of "Surprises" with Damage

First we identify the largest peaks in the square coefficients. By far the largest peak (see T1 in Fig. 9a) occurs at about 11.2 s in the NS acceleration of channel 9, on the 2^{nd} floor at the east end of the building, *consistent with the location of the most severe damage* (failure of the first story columns of frame F; see Fig. 4). This peak is more than an order of magnitude larger than all other peaks. There is also a large peak at this time in the NS acceleration on the roof at the east side of the building (T2), also consistent with the description of damage.

Next large magnitudes surprise, consistent with the damage, is T3, on the 2^{nd} floor at the west side of the building (channel 7) at about 6.3 s, followed by smaller surprises between 8.2 to 9.2 s after trigger, marked as T3a. Both are consistent with the reported smaller damage at the 2^{nd} floor at the west side of the building. Smaller surprises (T4) at about 6.3 s are also observed on the 2^{nd} floor at the center of the building (channel 8), followed by surprises T4a, which also can be related to reported damage in that part of the building. In these two channels, some small surprises are also seen within the third highlighted time interval. These are identified respectively by T3b and/or I-T1, and T4b and/or I-T1, and explained as possible additional local damage (to the one identified by surprises T3 and T4), or as an effect (or "influence") of the most severe damage identified by surprise T1, felt also at the center.

Within the first and second highlighted time intervals, smaller surprises are seen also in channel 9, preceding surprise T1. These are marked by T1a (at 6.8 s), and T1b (between 8.2 and 9.2 s). The former can be interpreted as initiation of the damage in the first story columns at the east side of the building, and the latter—as additional damage, leading to the failure of these columns at about 11.2 s, as indicated by surprise T1.

Next, we analyze the surprises in the roof response at the west side and at the center of the building (channels 1 and 2). Large surprises are observed at the west side of the building within the second highlighted time interval, and at the center of the building within the first highlighted interval. These cannot be related to severe reported damage, and hence are interpreted as "false positive" and marked by F1 and F2. The smaller surprises in these channels are interpreted as influences of damage that occurred further away from these sensors. In channel 1, these surprises are marked as I-T3 and I-T2, and interpreted to be possibly due to the damage identified by T3 and T2.

In the EW accelerations, which were recorded only at the center of the building, prominent "true" surprises are seen at about 11.2 s, on the 2^{nd} and 4^{th} floors, and at the roof, all consistent with the observed damage. Those observed at the 2^{nd} floor and roof are interpreted to be due to the damage identified by surprises T1 and T2 in the NS response, and are named by the same symbols as for the NS response. Surprises are also seen at the second floor, between about 5 and 7 s, interpreted to be due to the damage identified by surprises T3 and T4. At the roof, two "false positive" surprises are identified, F1 and F2.

The analysis of the surprises so far suggests that severe damage in this building started to occur at the west side of the building at about 6.4 s after trigger, and was most significant in the first story columns. The damage at the east side of the building started to occur later, at about 6.8 s after trigger. Additional severe damage occurred between 8.2 to 9.2 s, which further weakened the *building, and finally lead to failure of the first story columns at the east side of the building at about 11.2 s, which was felt throughout the building.*

4.2.2 Consistency of "Surprises" with Changes in System Frequency

The analysis of "surprises" in Section 4.2.1 indicated that the major damage occurred at about 6.4 s, 8.2–9.2 s, and 11.2 s. The plots of instantaneous frequency (Fig 5 and bottom of Fig. 9a,b) suggest that the NS frequency dropped from about 2 Hz in the early stage of response (at about 3 s) to about 1.55 Hz ($\Delta f = 0.45$ Hz or 22.5%), was constant in the interval 6.5–8 s, and further dropped to 0.8 Hz ($\Delta f = 0.75$ Hz or 48%) in the interval 8–12 s. The EW frequency dropped from 0.9 to 0.65 Hz ($\Delta f = 0.25$ Hz or 28%) in the interval 5–7 s, was approximately constant in the interval 7–9.5 s, and dropped gradually to 0.55 Hz ($\Delta f = 0.1$ Hz or 15%) in the interval 13–14 s. It is noted here that the estimation of the time of the change is limited by the finite time resolutions of the method. For this case (Gabor transform with $\sigma = 1$), an "instant" is the time interval $2\sigma_t$ = $2 * 0.71$ =1.4 s.

A comparison of the times and magnitudes of the drops in system frequency with the times and magnitudes of the "surprises" associated with damage shows that the most severe damage (failure of the first story columns at the east side of the building at 11.2 s) *cannot be identified from changes of the EW frequency*. The 48% drop of the NS frequency was most likely, at least in part, due to the structural damage. The timing of the occurrence of the damage can be estimated more precisely from the analysis of the "surprises."

4.2.3 Causality of the Detected "Surprises"

Next, we examine the causality of the surprises in different channels by measuring (approximately) the time lag between them. One objective of this analysis is to find out if the surprises on the roof can be explained by high frequency pulses of the input motion that have propagated through the building, and another objective is to find out how disturbances created by the occurrence of damage propagated through the structure and were "felt" at other locations. We start with a small surprise at 5.83 s, marked as G1 (see Fig. 9) and seen both in channels 10 and 11, which occurred before the amplitudes of response became large and significant damage started to occur. This surprise is apparently due to a pulse in the ground motion, and is seen (delayed) also in the 2nd floor and roof records both at the east and west sides of the building. At the west side of the building, the pulse at the roof is delayed by $\tau = 0.155$ s relative to the ground floor, which implies velocity of wave propagation in the vertical direction $c_z = H/\tau = 25.5/0.155 = 164.5$ m/s. For a fixed-base model of a building deforming in shear, level of fixity at the ground floor, and assuming that the first mode is a quarter of a wavelength, this wave velocity implies fixed-base frequency $f_{\mathrm{NS,fb}} = c_z / 4H$ = 164.5/(4*25.5) = 1.6 Hz. At the east side of the building, the time delay is about τ = 0.14 s, which implies velocity of propagation c_z=182 m/s, and fixed-base frequency 1.78 Hz. The average of these two values for the NS response is about 1.7 Hz, and is in agreement with the instantaneous frequency at 5.8 s estimated by the Gabor transform (1.6 Hz).

A comparison of the amplitudes of the surprises at the ground floor and at the roof implies energy of the pulse at the roof being about 1.5 times the energy at the ground floor, which is equivalent to amplitude amplification of 1.2 at the roof. This factor can be explained by reduction of amplitude to 0.6 of the amplitude of the input (see Gicev, 2005), followed by amplification by a factor of 2 due to reflection from the stress free top of the building.

Next we analyze the propagation of the pulse identified by surprise G2, which also appears to be due to a high frequency pulse in the input motion. This pulse arrived at the building site at about 6.3 s after trigger, has a much larger amplitude than pulse G1, and is concurrent with surprise T3 in channel 7 at the west side of the building, interpreted to have been caused by damage at the west side of the building. This pulse can be traced at the roof delayed by $\tau \approx$ 0.155 s both at the west and east sides of the building, which also implies vertical shear wave velocity of about c_z =165 m/s, and frequency 1.6 Hz. A comparison of the magnitudes of the surprises implies an overall reduction of the amplitude at the roof by a factor of about 0.8 at the west side and about 0.6 at the east side of the building. A possible explanation for the reduction of amplitude compared to the amplification in the case of G1 is that the damage started to occur concurrently with this pulse. The arrival of this pulse at the roof at the center of the building cannot be detected due to interference with false surprise F2, which occurred at a time almost twice the travel time of waves from the ground floor to the roof, and appears to have been caused by some source near the roof.

Similarly, we follow the propagation of the pulse identified at the ground floor by surprise G3, at 7.8 s after trigger clearly seen at the west side of the building. The travel time to the roof is about τ =0.18 s, which implies vertical shear wave velocity $c_z \approx 142$ m/s, and frequency ≈ 1.4 Hz, which is in qualitative agreement with the system frequency estimated by the Gabor transform. The amplitude of the surprises implies reduction of amplitude of the pulse by a factor ~0.5.

In contrast to surprises G1, G2 and G3, which were due to pulses in the ground motion and appear delayed at the upper floors, surprise I-T1 in channel 11 at the ground floor is delayed, by about 0.05 s, with respect to surprise T1 at the 2nd floor, and appears to be due to the disturbance caused by the failure of the first story columns at the east side of the building, which propagated through the building. This delay time of 0.05 s along distance of 5 m (height of the first floor) implies velocity of about 100 m/s. Surprise T2 identified at the east side of the roof occurs concurrently with T1, which implies that it is due to damage near the roof. The smaller surprise following T2, marked as I-T1, appears delayed relative to T1 by $\tau \approx 0.16$ s and is likely due to a disturbance created by the failure of the first story columns that propagated towards the roof.

A similar analysis of travel times of pulses of EW motion can also be done, e.g. for the ground motion pulse identified by surprise G1 at about 5.8 s, and for the disturbance created by the failure of the first story columns in frame F at about 11.2 s, identified by surprise, T1. Pulse G1 reached the roof with a delay of $\tau \approx 0.27$ s, which implies velocity of wave propagation $c_z \approx$ 94 m/s, and fixed base frequency $f_{\mathrm{EW,fb}} = c_z / 4H$ =0.92 Hz. The travel time of pulse T1 from the 2nd floor to the roof was $\tau \approx 0.32$, which implies wave velocity $c_z \approx$ 64 m/s between the 2nd floor and roof, and, if extrapolated to the first story, implies frequency $f_{\mathrm{EW,fb}} = 0.63$ Hz. Although the time delays were measured only approximately, the EW frequencies they imply agree very well with the estimates of instantaneous frequency by the Gabor transform.

The above analysis suggests that *travel times of high frequency pulses propagating through the building can be measured using wavelet decomposition and used to estimate the shear wave velocity in the building*, *which can be done even for complex excitation such as strong ground motion, with further complications caused by the occurrence of damage.* The precision of such an analysis could be improved by using wavelets with a more compact support, and possibly by using controlled excitation, in which case it may possible to detect damage in columns from changes in travel time. Such detailed analysis is beyond the scope of this study.

Further details about this study, such as application to different measures of absolute and relative response, besides acceleration can be found in Todorovska and Trifunac (2005).

4.0 CONCLUSIONS

The analysis of surprises in the response of the Imperial County Services building to the 1979 Imperial Valley earthquake, which severely damaged the building, showed that: (1) this method, applied to the acceleration records, could identify the time of occurrence and general location of the major damage (with spatial resolution equal to the spacing of the sensors), and (2) the relative magnitudes of the surprises were proportional to the degree of damage. (3) This method was more effective in the analysis of NS response than in the analysis of the EW response, as the former was recorded by a spatially denser array - along three vertical lines, while the latter was recorded only along one line – at the center of the building. It is also possible that his was in part due to the larger flexibility of the building in the EW direction, which calls for further investigations of the effect of the building flexibility on the magnitudes of the surprises.

6.0 REFERENCES

1. Chang P.C., Flatau A., Liu S.C. (2003). "Review paper: health monitoring of civil infrastructure," Structural Health Monitoring, 2(3), 257-267.

2. Corbin M, Hera A and Hou Z (2000). "Locating damage regions using wavelet approach," Proc. Fourteenth Engineering Mechanics Conference, ASCE. Department of Civil Engineering, May 22-24, University of Texas at Austin.

3. Doebling S.W., Farrar C.R., Prime M.B., Shevitz D.W. (1996). "Damage identification and health monitoring of structural and mechanical systems from changes in their vibration characteristics: a literature review," Report LA-13070-MS, Los Alamos National Laboratory, Los Alamos, NM.

4. Gicev V. (2005). "Investigation of soil-flexible foundation-structure interaction for incident plane SH waves," Ph.D. Thesis, University of Southern California, Dept. of Civil Engineering.

5. Hera A., Hou Z. (2004). "Application of wavelet approach for ASCE structural health monitoring benchmark studies," J. of Eng. Mech., ASCE, 130(1), 96-104.

6. Hou Z., Noori M., Amand R. (2000). "Wavelet-based approach for structural damage detection," J. Eng. Mech., ASCE. 126(7), 677-683.

7. Ivanović S., Trifunac M.D., Novikova E.I., Gladkov A.A., Todorovska M.I. (2000). "Ambient vibration tests of a seven-story reinforced concrete building in Van Nuys, California, damaged by the 1994 Northridge Earthquake," Soil Dynamics and Earthquake Engrg, 19(6), 391-411.

8. Jordanovski L.R., Trifunac, M.D. (1990). "Least square model with spatial expansion: application to the inversion of earthquake source mechanism," Soil Dynamics and Earthquake Engineering, 9(6), 279-283.

9. Jordanovski L.R., Trifunac, M.D. (1990). "Least square inversion with time shift optimization and an application to earthquake source mechanism," Soil Dynamics and Earthquake Engineering, 9(5), 243-254.

10. Kojić S., Trifunac M.D., Anderson J. C. (1984). "A post earthquake response analysis of the Imperial County Services building in El Centro," Report CE 84-02, University of Southern California, Department of Civil Engineering, Los Angeles, CA.

11. Mallat S.G. (1989). "Multiresolution approximations and wavelet orthonormal bases of $L_2(R)$," Trans. Amer. Math. Soc, 315, 69-87.

12. Ovanesova A.V., Suárez L.E. (2004). "Applications of wavelet transform to damage detection in frame structures," Engineering Structures, 26, 39-49.

13. Pardoen, G.C. (1979). "Imperial County Services Building: Ambient vibration tests results," Report 79-14, Dept. f Civil Eng., Univ. of Canterbury, New Zealand.

14. Rezai M., Rahmatian P., Ventura C. (1998). “Seismic data analysis of a seven-storey building using frequency response function and wavelet transform”. Proc. of the NEHRP Conference and Workshop on Research on the Northridge, California Earthquake of January 17, 1994. Vol. III. pp. 421-428, CUREe, Oakland, CA.

15. Sohn H, Law K. (1999). “A Bayesian probabilistic approach to damage detection for civil structures,” Report No. 131, Dept. of Civil and Environmental Engineering, Stanford University, Palo Alto, CA.

16. Sone A., Yamamoto S., Nakaoka A., Masuda A. (1995). “Health monitoring system of structures based on orthonormal wavelet transform,” Seismic Engineering, ASME, 312, 161-167.

17. Todorovska M.I., Lee V.W. (1989). “Seismic waves in buildings with shear walls or central core,” J. Engrg Mech., ASCE, 115 (12), 2669-2686.

18. Todorovska M.I. (2001). “Estimation of instantaneous frequency of signals using the continuous wavelet transform,” Report CE 01-07, Dept. of Civil Engrg., Univ. of Southern California, Los Angeles, California, pp. 55.

19. Todorovska M.I., Hao T.-Y. (2003). “Information granulation and dimensionality reduction of seismic data vibration monitoring data using orthonormal discrete wavelet transform for possible application to data mining,” Report CE 03-02, University of Southern California, Department of Civil Engineering, Los Angeles, CA.

20. Todorovska M.I., Trifunac M.D. (2005). “Structural health monitoring by detection of sudden changes in recorded seismic response using discrete wavelet transform—application to a 6-story RC building,” Report CE 05-01, University of Southern California, Dept. of Civil Engineering, Los Angeles, CA. (draft).

21. Trifunac M.D., Lee V.W. (1979). “Automatic digitization and processing of strong motion accelerograms.” Parts I and II, Dept. of Civil Eng. Report No. 79-15, Univ. of Southern California, Los Angeles, California.

22. Trifunac M.D., Todorovska, M.I. (2001). “Recording and interpreting earthquake response of full-scale structures,” in M. Erdik, M. Celebi, V. Mihailov, and N. Apaydin (Eds.), *Proc. NATO Advanced Research Workshop on Strong-Motion Instrumentation for Civil Engineering Structures*, June 2-5, 1999, Istanbul, Turkey, Kluwer Academic Publishers, 2001, pp. 24.

23. Trifunac M.D., Ivanović S.S., Todorovska M.I. (2001). “Apparent periods of a building I: Fourier analysis,” J. of Struct. Engrg, ASCE, 127(5), 517-526.

24. Trifunac M.D., Ivanović S.S., Todorovska M.I. (2001). “Apparent periods of a building II: time-frequency analysis,” J. of Struct. Engrg, ASCE, 127(5), 527-537.

25. Vetterli M., Kovacević, J. (1995). “Wavelets and subband coding,” Prentice Hall PTR, Upper Saddle River, NJ.

26. Vincent H.T., Hu S.-L., Hou Z. (1999). “Damage detection using empirical mode decomposition method and a comparison with wavelet analysis,” Proc. 2nd International Workshop on Structural Health Monitoring. Stanford University, Stanford, California. September 8-10.

27. Wang Q., Deng X. (1998). “Damage detection with special wavelets,” Int. J. of Solids and Structures, 36, 3443-3468.

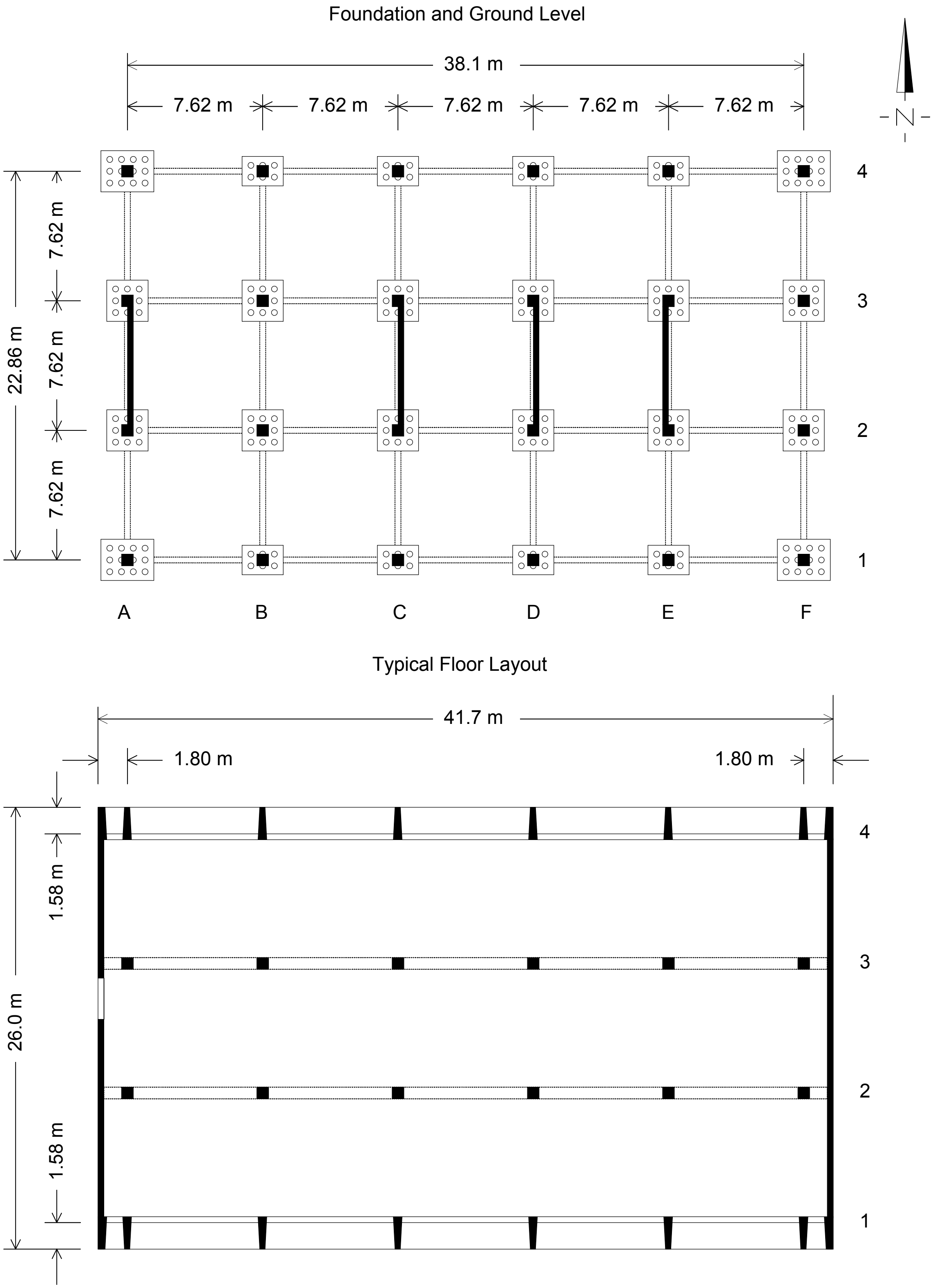

Figure 1: Foundation and ground level plan and typical floor layout of the ICS building.

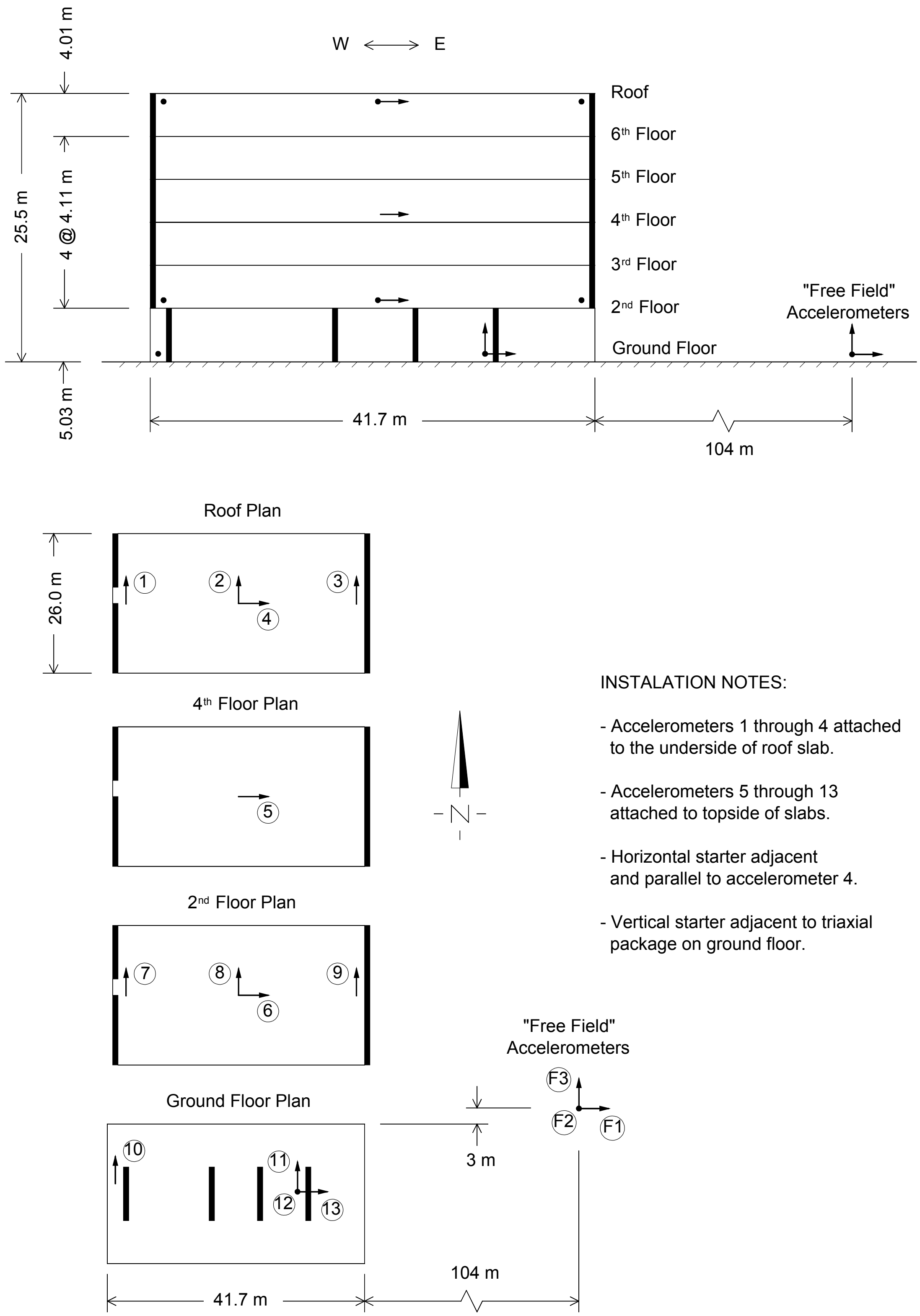

Figure 2: A layout of the seismic monitoring array in the ICS building.

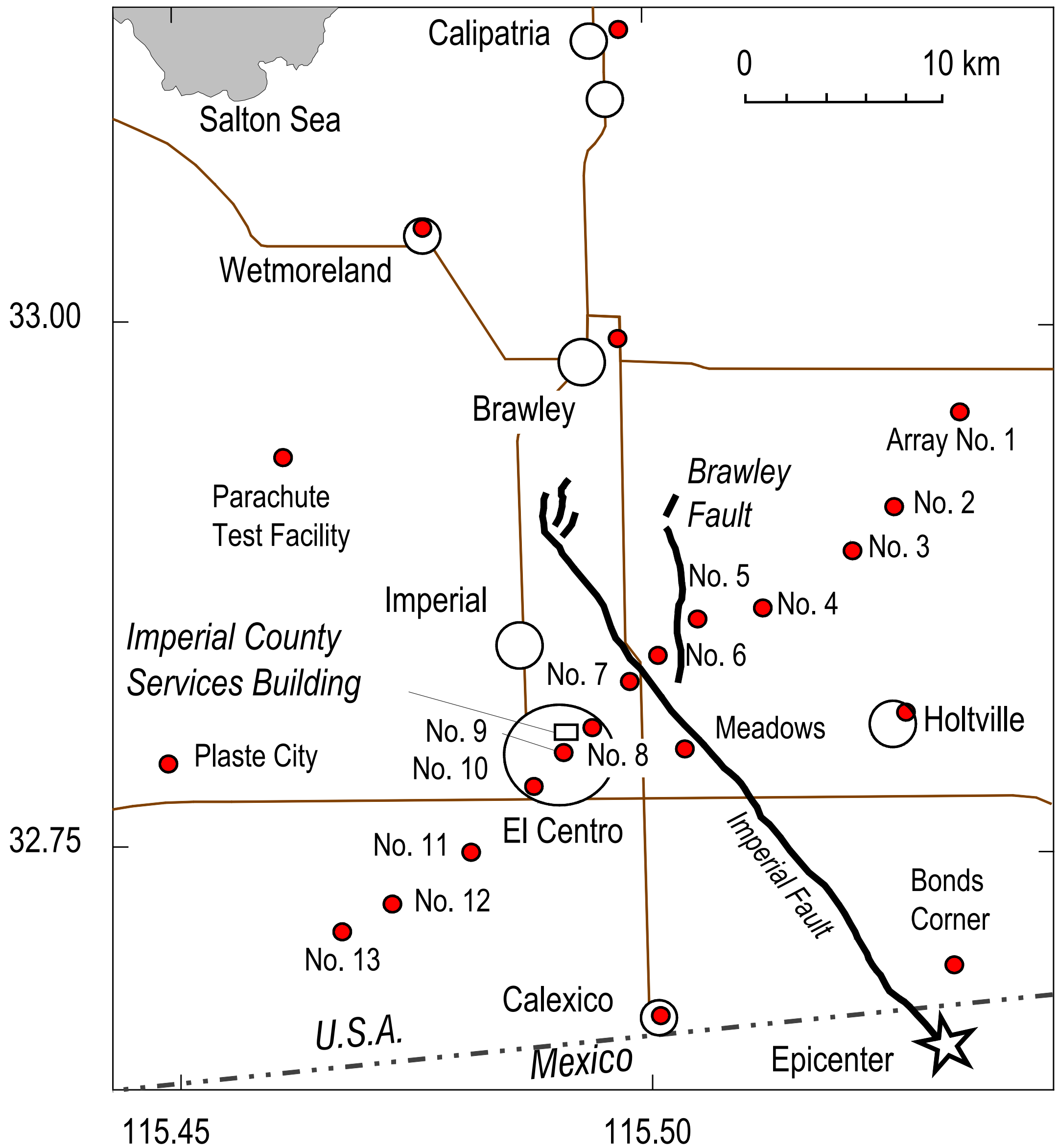

Figure 3: Location of the Imperial Fault relative to the site of the ICS building and strong motion stations in Imperial Valley.

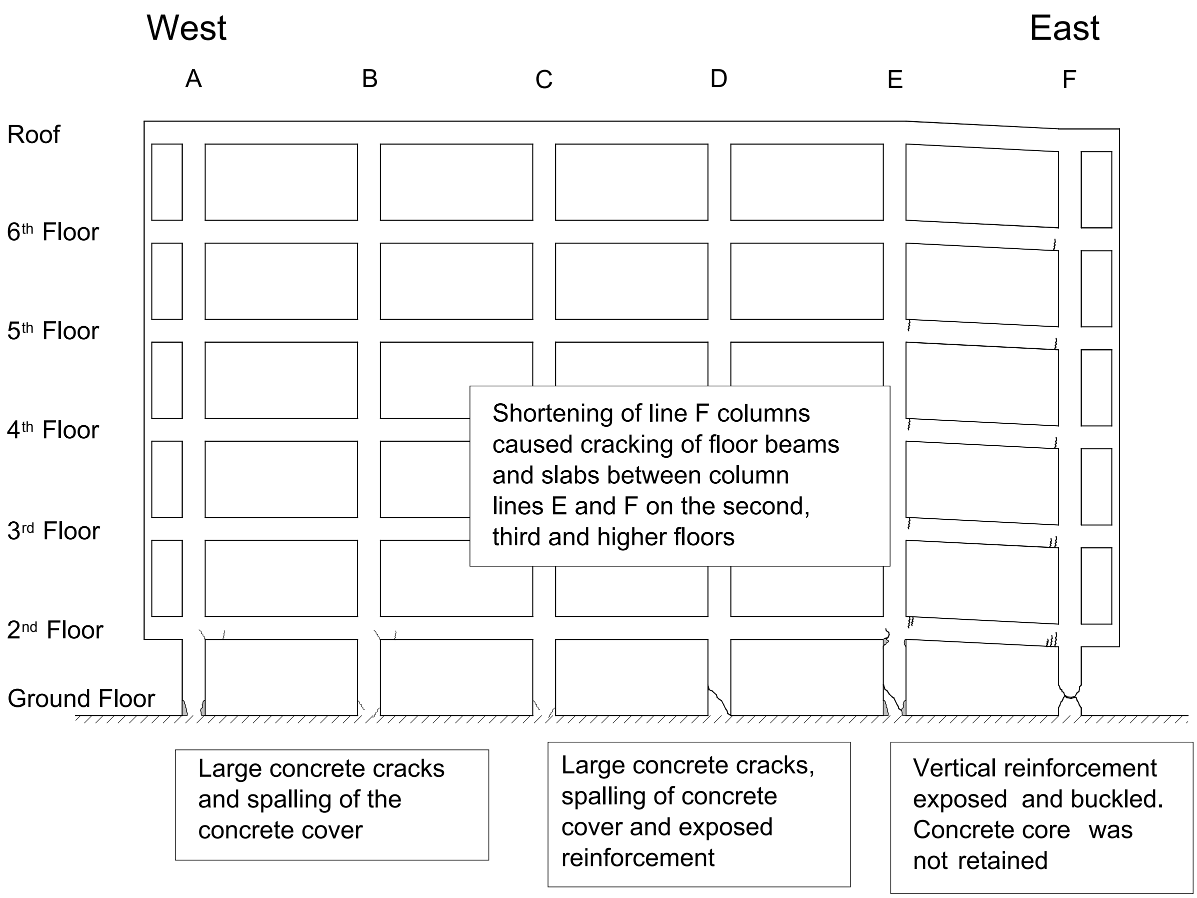

Figure 4: Schematic representation of the damage in the ICS building following the 1979 Imperial Valley earthquake.

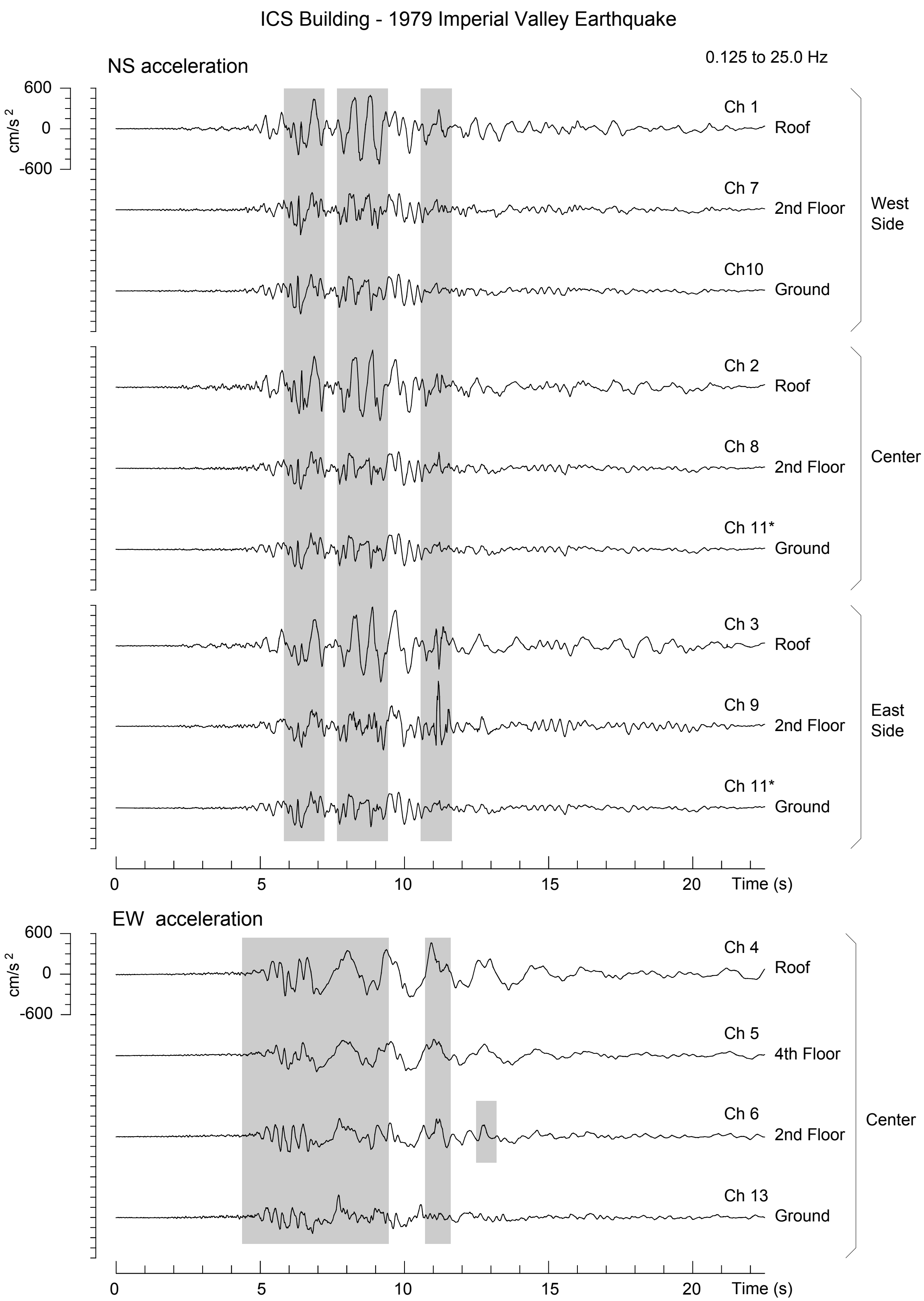

Figure 5: Accelerations (NS and EW components) recorded in the ICS building during the 1979 Imperial Valley earthquake.

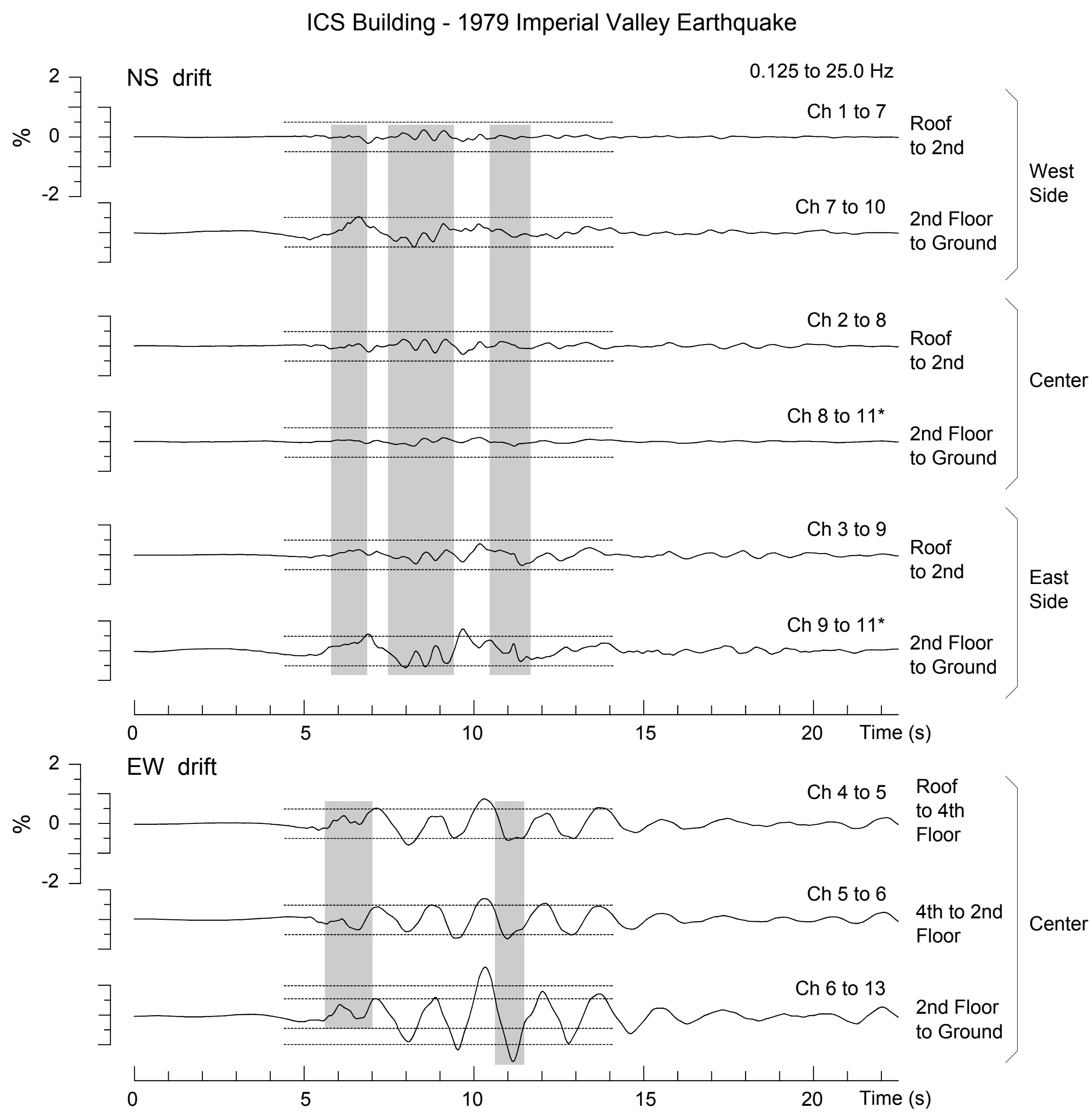

Figure 6: Inter-story drifts in the ICS building during the 1979 Imperial Valley earthquake. The horizontal lines mark 5% and 10% drift levels.

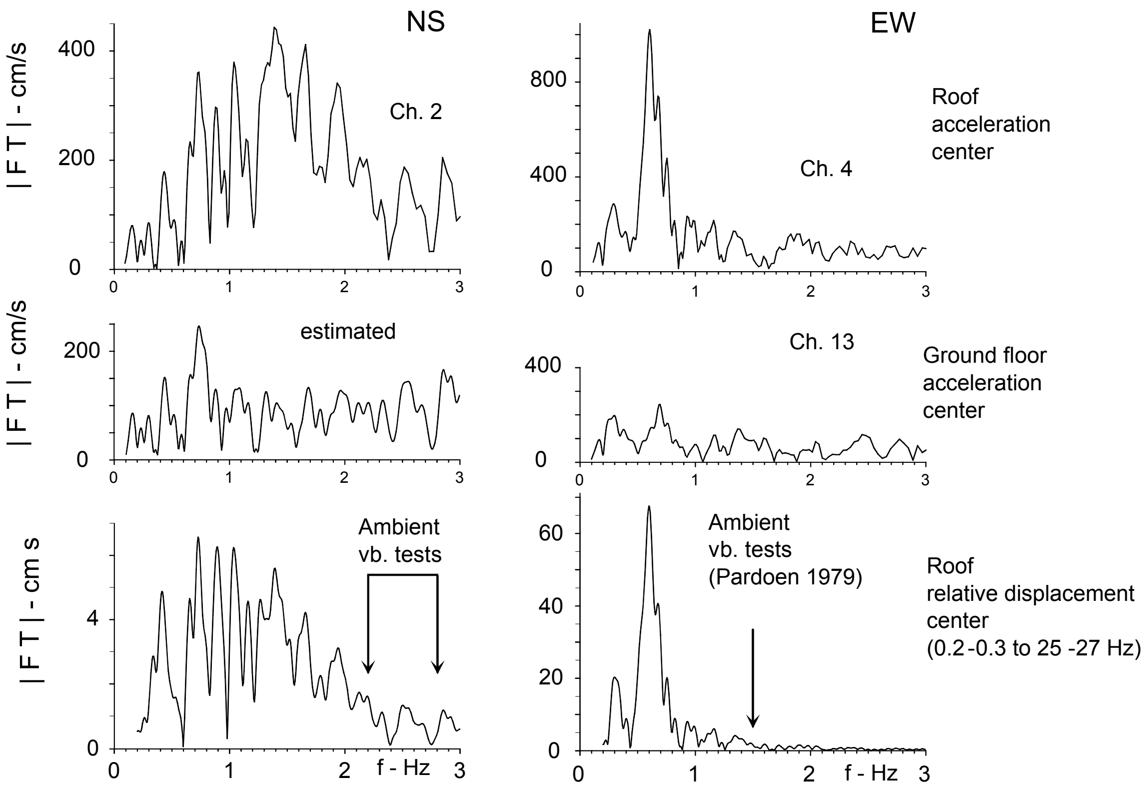

Figure 7: Fourier transform amplitudes of NS (left) and EW (right) response of the Imperial County Services Building to the 1979 Imperial Valley earthquake: roof acceleration (top), ground floor acceleration (middle) and relative displacement (bottom), at the center of the building.

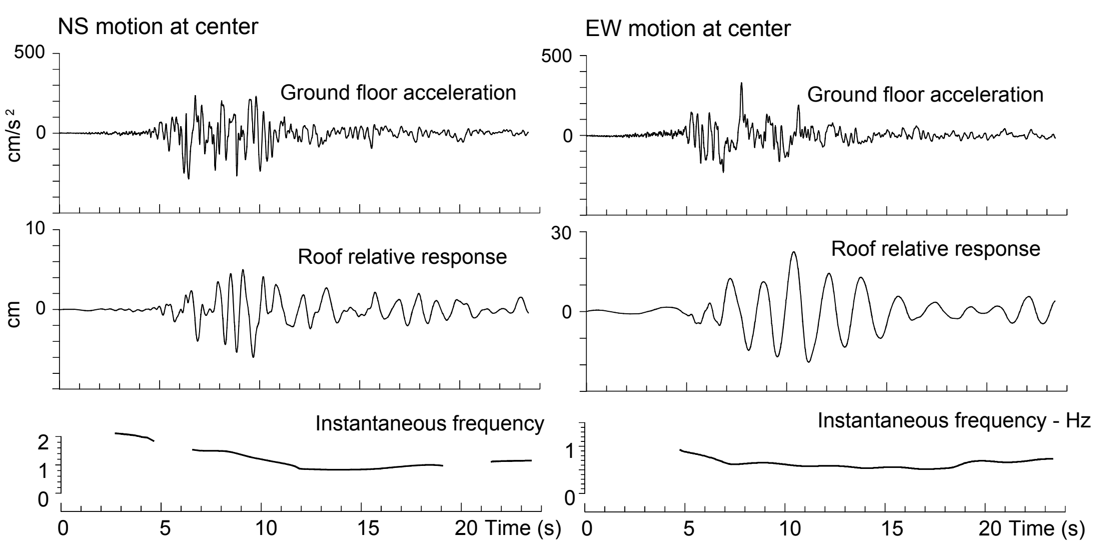

Figure 8: Time histories of NS (left) and EW (right) responses of the Imperial County Services Building to the 1979 Imperial Valley earthquake: (top) ground floor acceleration, (middle) roof displacement at the center of the building relative to the ground floor response, and (bottom) system frequency.

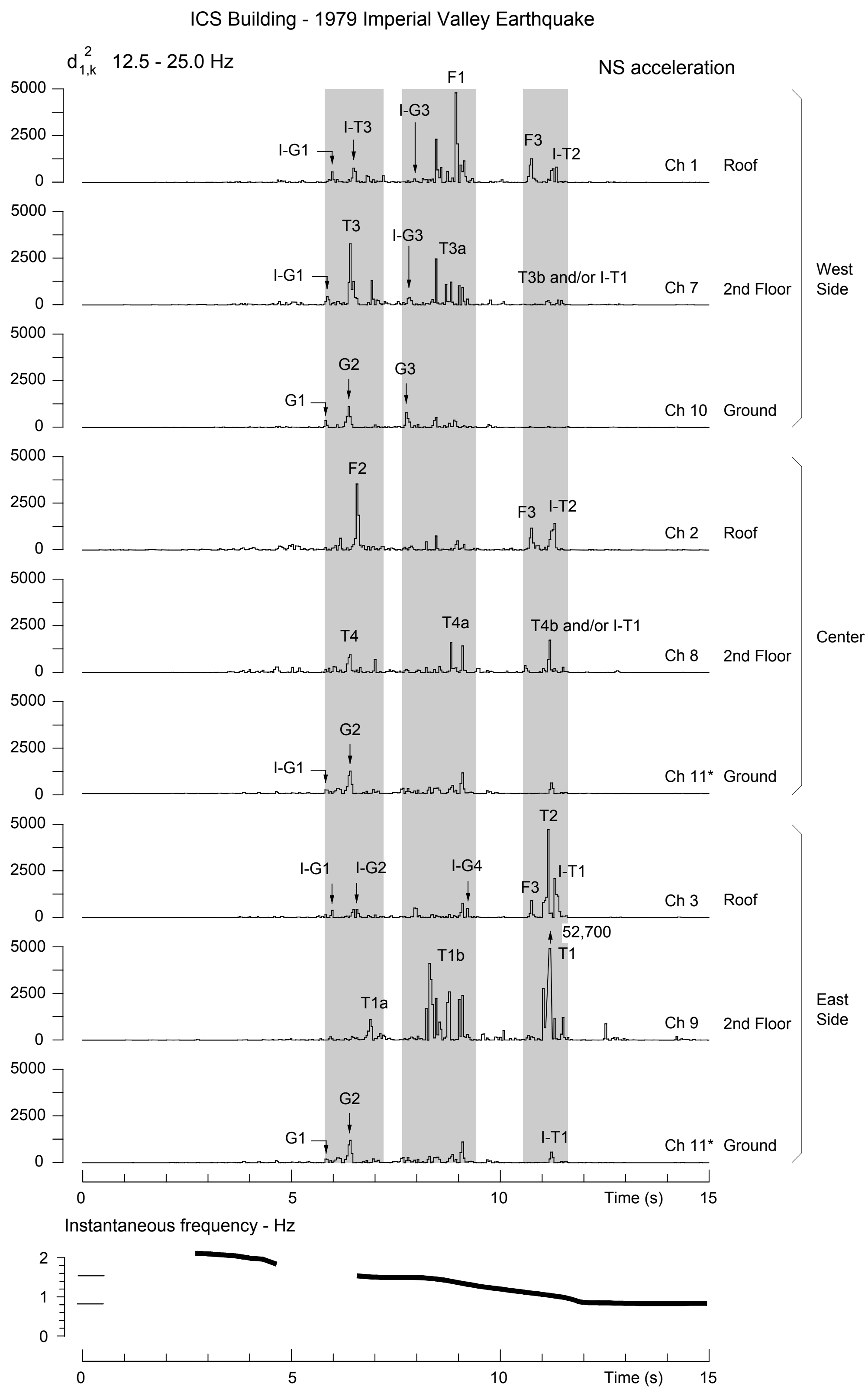

Figure 9a Squared coefficients of NS acceleration in subband 12.5-25 Hz (top) and instantaneous frequency (bottom).

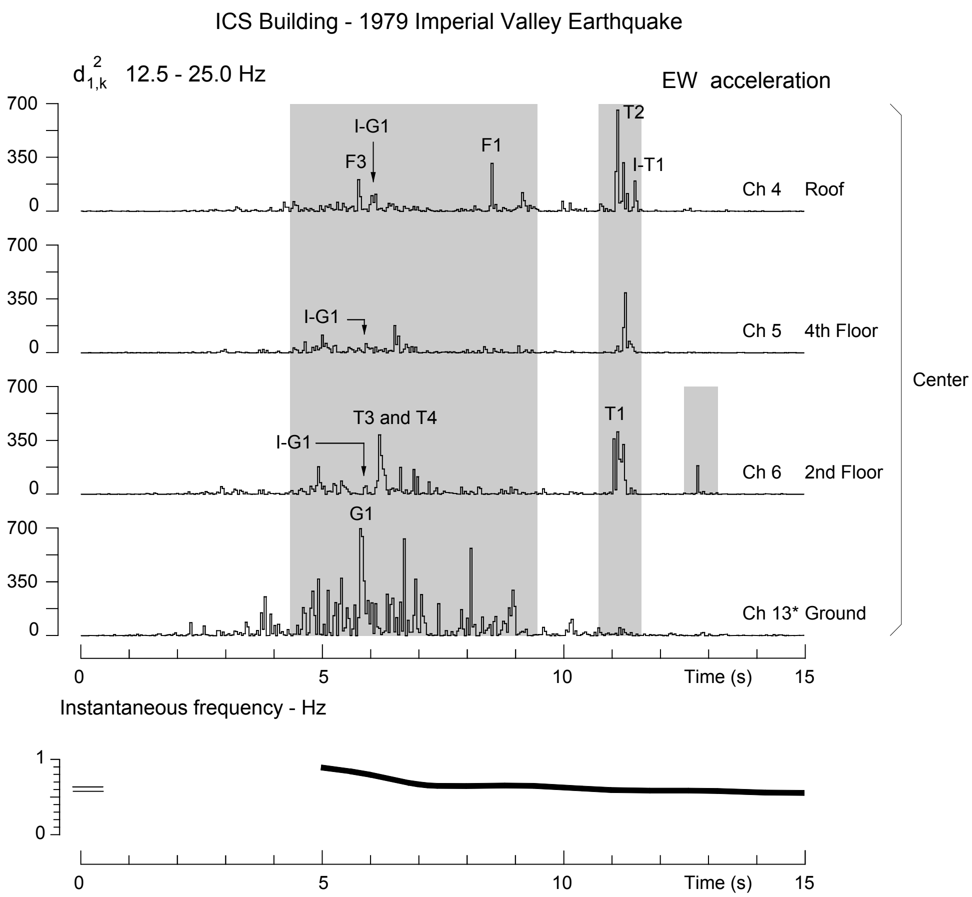

Figure 9b Squared coefficients of EW acceleration in subband 12.5-25 Hz (top) and instantaneous frequency (bottom).